

Integrating Physics-Informed Deep Learning and Numerical Methods for Robust Dynamics Discovery and Parameter Estimation

Caitlin Ho, Andrea Arnold*

Department of Mathematical Sciences, Worcester Polytechnic Institute, Worcester, MA, USA

* Corresponding author: anarnold@wpi.edu, ORCID 0000-0003-3003-882X

Abstract

Incorporating a priori physics knowledge into machine learning leads to more robust and interpretable algorithms. In this work, we combine deep learning techniques and classic numerical methods for differential equations to solve two challenging problems in dynamical systems theory: dynamics discovery and parameter estimation. Results demonstrate the effectiveness of the proposed approaches on a suite of test problems exhibiting oscillatory and chaotic dynamics. When comparing the performance of various numerical schemes, such as the Runge-Kutta and linear multistep families of methods, we observe promising results in predicting the system dynamics and estimating physical parameters, given appropriate choices of spatial and temporal discretization schemes and numerical method orders.

Keywords: scientific machine learning, dynamical systems, inverse problems, system identification, parameter estimation, missing physics

MSC Codes: 68T07, 68T20, 65L09, 65M32

1 Introduction

Mathematical modeling often involves examining the key attributes of dynamical systems that can be used to explain and predict the behavior of many real-world phenomena. Two important aspects of this process, system identification and parameter estimation, aim to improve our understanding of the system dynamics through use of observed data. Recently, a growing number of proposed methods numerically approximate the system dynamics directly from observed data [1–3]. Dynamics discovery can be considered as a function approximation problem by treating the unknown governing equations as target functions dependent on the system states and time derivatives. This problem has been explored in the context of both

ordinary differential equations (ODEs) [2, 4, 5] and partial differential equations (PDEs) [3, 6–8]. Furthermore, there has been increased interest in combining scientific knowledge with machine learning (ML) to create more robust and interpretable algorithms in the emerging field of scientific machine learning (SciML) [9–12].

In this work, we introduce a novel SciML approach that combines deep learning and numerical methods to address system identification and parameter estimation problems in deterministic dynamical systems. There are various approaches in the literature that combine scientific knowledge and ML. One approach enforces domain knowledge into ML to constrain the set of possible approximate functions [6, 8, 13]. Another perspective utilizes ML to discover new domain knowledge by learning from an undefined system [1, 3, 14]. Within this framework, we consider how to incorporate ML into scientific computing with the goal of improving dynamical system predictions by (i) enforcing physics in cases where it is known and (ii) augmenting with ML in cases where it is unknown.

When we know the physics governing a dynamical system, a common strategy in SciML is to ensure alignment with the underlying physics. The work of Raissi, Perdikaris, and Karniadakis (2019) proposed a data-driven solution for both continuous and discrete time models using a physics-informed neural network (PINN) that considers the forward problem of solving a given PDE and a discovers unknown parameters for the inverse problem [6]. PINNs encode the known PDE into a neural network loss function to learn the PDE solution. Many works have since applied PINNs to various problems and fields of study [6, 8, 10, 11, 13, 15], in some cases optimizing the PINNs for use in specific applications such as problems with multi-scale solutions or complex-geometry domains [16–19].

To address the two problems of interest in this work, we consider hybrid methods that combine PINNs with traditional numerical methods for solving ODEs. Previous works have incorporated numerical methods into PINN methodology by replacing automatic differentiation with numerical differentiation schemes, such as finite difference methods [20, 21]. Another hybrid modeling approach incorporates the PINN within an iterative scheme to refine and improve the numerical solution to linear systems and ODEs [22, 23]. Note that both PINNs and numerical methods require that the governing equations are known, essentially acting as iterative solvers to update the numerical approximation at each time step. However, in many applications, the idea of *missing physics* is prevalent: Often, the equations governing a dynamical system are either completely unknown or partially known. Instead of the existing hybrid methods that compute or refine solutions to the forward problem, we consider the question of whether traditional numerical methods can be coupled with a neural network to recover varying degrees of missing physics in addressing system identification and parameter estimation problems.

System identification aims to discover the unknown dynamics of a system using only observed data from that system. In real-world applications, the observed data are typically limited (i.e., not all system components are observed) and noisy. System identification problems can result in equation discovery by finding an approximate representation of the governing equations [1, 24] or dynamics discovery by determining an approximation of the dynamics [3, 14, 25]. Equation discovery requires prior knowledge of candidate functions to learn the unknown weights of each of these terms and build the governing equations, which is feasible in some applications where the physics or underlying scientific knowledge is well studied. However, unlike the approach in [1], in this work, we do not assume that we have

an understanding of candidate functions that could be included in the governing equations and, instead, learn the system dynamics solely from data. In fact, we do not discover the governing equations explicitly but implicitly determine an approximation of the dynamical system for prediction.

Parameter estimation, the inverse of the forward prediction problem, aims to estimate the physical parameters of the system, given the available system observations, which are most often noisy and limited. There are a variety of deterministic and statistical methods in the literature to estimate system parameters when the governing equations are known; see, e.g., [26–36]. In the deep learning setting, some approaches use a neural network approximation for the physical parameters [5, 37] while others add the physical parameters to the neural network to be optimized along with the weights and biases [6, 38]. The parameter estimation problem can be viewed as the middle ground between the forward prediction and system identification problems: Here, we know the functional form of the governing equations but estimate the unknown physical parameters using ML with observed data from the system.

Another related facet of SciML, termed differentiable physics, aims to improve numerical solvers by incorporating robust ML methods and differentiable programming [39–42] into various modeling steps, particularly in areas with uncertainties or where traditional methods are computationally expensive [43–47]. As a prime example of this approach, neural ODEs combine neural networks with traditional numerical methods for ODEs to learn the underlying system dynamics [25]. Neural ODEs have been applied to many problems including normalizing flows [48], image classification [49, 50], and learning dynamics from partially-observed systems [14, 51, 52]. Universal differential equations expand upon the neural ODE to define a universal framework for SciML that approximate unknown physics with a neural network [46]. While both neural and universal ODEs seamlessly integrate neural network approximations into numerical solvers, the resulting approximations do not explicitly enforce physics-informed constraints in the loss function.

1.1 Contributions

In this work, we extend ideas from PINNs [6] and neural ODEs [25] to develop a robust computational framework that combines a constrained neural network, akin to a PINN, with an iterative numerical scheme similar to a neural ODE. Most existing works on PINNs and neural ODEs assume that the observed data are either contaminated with weak Gaussian noise or no noise at all. Several approaches assume Gaussian noise in the context of sparse and irregular data [24, 53] or uncertainty quantification [54] while others consider non-Gaussian noise [55]. We consider the case of uniformly observed data corrupted with significant Gaussian noise. This framework effectively combines deep learning and classic numerical methods to address dynamics discovery and parameter estimation problems given corrupt system observations. In both problems of interest, the missing information inhibits the naive implementation of a numerical method or neural network independently for the problem. Thus, we propose combining these two approaches, allowing for convergence to a solution from the numerical method while also incorporating the flexibility of a data-driven approach. We provide two main contributions to address missing physics problems in the setting of dynamical systems with noisy data:

- We combine neural networks and traditional numerical schemes to solve differential equations in a novel architecture for learning completely unknown system dynamics. In particular, we use a neural network to approximate the unknown dynamics and train the neural network with a numerical approximation of the states and observed data from the system.
- We use a similar architecture and loss function to address the parameter estimation inverse problem and learn the unknown physical parameters of a system. We generate a neural network approximation of the states at discretized time steps and train the neural network in two phases. We use a numerical scheme with randomly initialized physical parameter values to pre-train the neural network. We then fine-tune the neural network to learn the unknown physical parameters using observed data from the system. Computational analysis highlights the importance of pre-training in enhancing the neural network’s approximation by properly initializing its parameters.

In both approaches, we augment traditional ODE solvers with neural networks to learn unknown system dynamics and physical parameter values. For dynamics discovery, we adopt a similar approach as the neural ODE [25] and its stochastic equivalent [56] by using a neural network to approximate the right-hand side (RHS) vector and implementing an ODE solver to train the neural network. However, our approach computes loss terms that not only minimize the squared ℓ^2 -norm with respect to the observed and predicted RHS dynamics, like in a neural ODE, but also with respect to observed data and computed states from the ODE solver. This constrains the solution set, similar to a PINN, by encoding the known physics—specifically, the observed dynamics and initial conditions—into the loss function. Further, while neural ODE approaches employ the adjoint sensitivity method [57] for computing the gradients, our proposed approach exploits automatic differentiation [47]. For parameter estimation, we implement a similar approach to the inverse problem using a PINN [6] as we augment the unknown physical parameters to the set of trainable parameters in the neural network for optimization. However, we employ this idea within the framework of differentiable physics by integrating the neural network within a traditional numerical method, like in the dynamics discovery problem.

1.2 Paper Organization

The remainder of the paper is organized as follows. Section 2 details the approaches for dynamics discovery and parameter estimation in this framework, and Section 3 applies these methods to a suite of nonlinear test problems that exhibit oscillatory and chaotic dynamics. Section 4 provides a discussion of results and concludes the paper with future considerations.

2 Methods

We consider dynamical systems of the form

$$\frac{d\mathbf{x}}{dt} = \mathbf{f}(t, \mathbf{x}; \lambda), \quad \mathbf{x}(t_0) = \mathbf{x}_0 \tag{2.1}$$

where $\mathbf{x} = \mathbf{x}(t) \in \mathbb{R}^n$ is a vector representing the states of the system at time t , the RHS function $\mathbf{f} : \mathbb{R} \times \mathbb{R}^n \times \mathbb{R}^{|\lambda|} \rightarrow \mathbb{R}^n$ is a mapping describing the system dynamics, and $\lambda \in \mathbb{R}^{|\lambda|}$ is a vector of the system physical parameters. Here, $|\lambda|$ denotes the number of physical parameters. We assume that $t_0 = 0$ and $\mathbf{x}_0 \in \mathbb{R}^n$ is a given initial condition.

In this paper, we aim to learn either the unknown dynamics \mathbf{f} or unknown physical parameters λ , given corrupt observations of the system states $\mathbf{x}(t)$ at some discrete times. To this end, we approximate the states of the dynamical system using the observed data. For dynamics discovery, we rely solely on observed data, whereas for parameter estimation, we assume the governing equations are known. We obtain this approximation of the system dynamics and physical parameters using feed-forward neural networks. Each layer besides the output layer uses $\sigma = \tanh(x)$ as the activation function. We use Adam [58] followed by L-BFGS [59] as the optimization algorithm for computational efficiency. More specifically, we apply an Adam optimizer with an initial learning rate of 0.001, followed by the L-BFGS optimizer with a learning rate of 1.0 and a maximum number of iterations of 50,000. As described further in Section 3, each application of these methods uses a different architecture of hidden layers and hidden nodes depending on the complexity of the problem.

2.1 Dynamics Discovery

The goal of dynamics discovery is to determine an approximation for the system dynamics that can be used for prediction. That is, we approximate the unknown RHS dynamics \mathbf{f} with a vector $\hat{\mathbf{f}} \in \mathbb{R}^n$ at some discretized time steps $t \in \mathbb{R}$, given the observed data from the system, denoted \mathbf{X}_{obs} . We learn the unknown dynamics \mathbf{f} by using a feed-forward neural network with the observed states as input. We then compute a numerical approximation of the states \mathbf{X}_{NM} using the neural network output $\hat{\mathbf{f}}_{DNN}$ and utilize the observed and approximated states in the loss function to update the RHS dynamics $\hat{\mathbf{f}}_{DNN}$. To train the neural network, we consider the following loss function:

$$\mathcal{L}(\theta) = \mathcal{L}_{ic}(\theta) + \mathcal{L}_p(\theta) + \mathcal{L}_d(\theta) \quad (2.2)$$

where

$$\mathcal{L}_{ic}(\theta) = \frac{1}{N_{ic}} \|\mathbf{X}_{NM}(t_0; \theta) - \mathbf{X}_0(t_0)\|_2^2 \quad (2.3)$$

$$\mathcal{L}_p(\theta) = \frac{1}{N_p} \|\hat{\mathbf{f}}_{DNN}(t; \theta) - \mathbf{f}_{obs}(t)\|_2^2 \quad (2.4)$$

$$\mathcal{L}_d(\theta) = \frac{1}{N_d} \|\mathbf{X}_{NM}(t; \theta) - \mathbf{X}_{obs}(t)\|_2^2 \quad (2.5)$$

and the vector θ contains the neural network weights and biases. Here, $\|\cdot\|_2^2$ denotes the square of the ℓ^2 -norm. All the above terms are written in vector notation, so \mathbf{X}_0 indicates a vector of the initial conditions, and \mathbf{X}_{NM} denotes the approximate solution given from the numerical schemes. Equation (2.3) indicates the initial condition loss comparing the given initial conditions from the problem with the numerical approximation of the states at $t = 0$. The physics loss in (2.4) compares the neural network output $\hat{\mathbf{f}}_{DNN}$ with \mathbf{f}_{obs} , which is computed from \mathbf{X}_{obs} using finite difference approximation. The data loss term in (2.5) accounts for differences in the approximated states \mathbf{X}_{NM} and the observed states \mathbf{X}_{obs} .

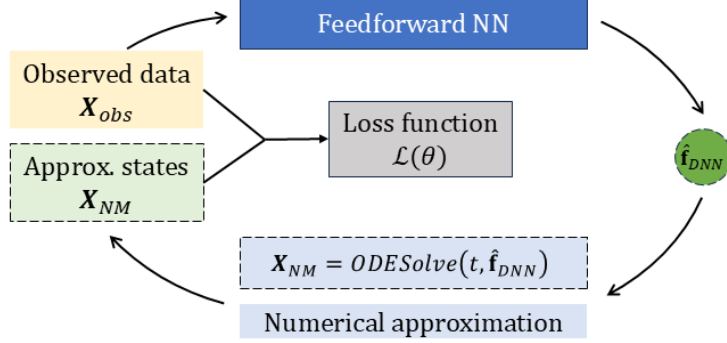


Figure 1: Schematic for the proposed neural network with numerical ODE methods to model dynamical systems with completely unknown dynamics. We obtain an approximation for the RHS dynamics $\hat{\mathbf{f}}_{DNN}$ using the observed states as input, then use $\hat{\mathbf{f}}_{DNN}$ to compute a numerical approximation of the states \mathbf{X}_{NM} . The observed and approximated states are used in the loss function to update $\hat{\mathbf{f}}_{DNN}$.

During each epoch of training, the learned RHS dynamics $\hat{\mathbf{f}}_{DNN}$ updates with adjustments made through comparisons with \mathbf{f}_{obs} in the loss function. We use the neural network output to compute \mathbf{X}_{NM} . Following a similar notation from [25], we compute \mathbf{X}_{NM} as follows:

$$\mathbf{X}_{NM} = \text{ODESolve}(t, \hat{\mathbf{f}}_{DNN}) \quad (2.6)$$

where we utilize Runge-Kutta (RK) and linear multistep methods (LMMs) as our numerical ODE solvers. We consider both explicit and implicit methods to account for various types of problems that may be stiff and complex. For clarity, the numerical approximation \mathbf{X}_{NM} will be hereafter referred to as the model prediction in the dynamics discovery problem since it uses the neural network approximation of the RHS to compute the state variables. Figure 1 illustrates the interaction between the neural network output with the numerical method for dynamics discovery, and Algorithm 1 provides pseudocode for the neural network training.

2.2 Parameter Estimation

For parameter estimation, we aim to determine the value of unknown physical parameters given a complete functional form of the governing equations and observed data from the system. We generate a neural network approximation of the system states at discretized time steps and train the neural network to learn the unknown physical parameters using the governing equations that describe the RHS dynamics. However, unlike the forward prediction problem considered in [6], here the RHS vector includes error from the estimated physical parameter values $\hat{\lambda} \in \mathbb{R}^{|\lambda|}$. We begin by pre-training the neural network with randomly initialized values for the physical parameters and then fine-tune the physical parameter approximations along with the neural network parameters. Since we assume the physical parameter values are unknown and the observed data are significantly noisy, pre-training the neural network parameters provides a better starting point for the neural network that is then refined during fine-tuning to perform the physical parameter estimation.

Algorithm 1 Neural network training for completely unknown dynamics

Input: Observed values from system \mathbf{X}_{obs} , initial conditions \mathbf{X}_0

Output: RHS approximation $\hat{\mathbf{f}}_{DNN}$ at time steps t

Define an optimizer *optim*

while *optim* tolerance not met **do**

 Reset gradients of *optim*

$\hat{\mathbf{f}}_{DNN} = DNN(\mathbf{X}_{obs})$

 Compute required gradients of \mathbf{X}_{obs}

 Compute $\mathbf{X}_{NM} = \text{ODESolve}(t, \hat{\mathbf{f}}_{DNN})$

 Compute initial condition loss: $\mathcal{L}_{ic}(\theta) = \frac{1}{N_{ic}} \|\mathbf{X}_{NM}(t_0; \theta) - \mathbf{X}_0(t_0)\|_2^2$

 Compute physics loss: $\mathcal{L}_p(\theta) = \frac{1}{N_p} \|\hat{\mathbf{f}}_{DNN}(t; \theta) - \mathbf{f}_{obs}(t)\|_2^2$

 Compute data loss: $\mathcal{L}_d(\theta) = \frac{1}{N_d} \|\mathbf{X}_{NM}(t; \theta) - \mathbf{X}_{obs}(t)\|_2^2$

$\mathcal{L}(\theta) = \mathcal{L}_{ic}(\theta) + \mathcal{L}_p(\theta) + \mathcal{L}_d(\theta)$

 Compute gradients of $\mathcal{L}(\theta)$ using backpropagation

 Update θ by taking an *optim* step

end while

We use the following general loss function in both phases of neural network training:

$$\mathcal{L}(\theta) = \mathcal{L}_{ic}(\theta) + \mathcal{L}_p(\theta) + \mathcal{L}_d(\theta) + \sum_{i=1}^{|\lambda|} \mathcal{L}_{\lambda_i} \quad (2.7)$$

where $\mathcal{L}_{ic}(\theta)$, $\mathcal{L}_p(\theta)$, and $\mathcal{L}_d(\theta)$ represent the initial condition, physics, and data loss terms, respectively, and each \mathcal{L}_{λ_i} is a parameter loss term enforcing a range of values for each system parameter λ_i , $i = 1, \dots, |\lambda|$. The work of Wang, Teng, and Perdikaris (2021) discovered a bias toward the physics loss term of a PINN due to vanishing gradients associated with the boundary loss term [15]. As a result, we chose our optimization algorithm very carefully since our proposed approaches implement a constrained loss similar to a PINN. We employ different training strategies for pre-training and fine-tuning. Pre-training uses an Adam optimizer with initial learning rate of 0.001, followed by L-BFGS optimizer with maximum number of iterations of 20,000. For fine-tuning, we utilize the same optimization procedure (Adam followed by L-BFGS) but with a smaller initial learning rate of 0.0001 and smaller maximum iteration of 5,000. To account for the vanishing gradient of the initial condition loss term in the fine-tuning phase of our approach, we add a weight of 10^3 in front of our initial condition loss term to improve neural network training.

2.2.1 Pre-training Phase

To begin the pre-training phase, we randomly initialize the physical parameter values by drawing each from a uniform distribution with lower and upper bounds set to enforce a likely range of values for the parameter. We then compute a numerical approximation \mathbf{X}_{NM} for the states at the discretized time steps using these parameter values in the known RHS, implicitly encoding the governing equations of the system, and compare this with the neural network output \mathbf{X}_{DNN} . This pre-training procedure prepares the neural network for

Algorithm 2 Neural network pre-training with uniform random initial physical parameters

Input: Discretized time steps t , initial conditions \mathbf{X}_0

Output: State approximation \mathbf{X}_{DNN} at time steps t , pre-trained network parameters θ

Define an optimizer $optim$

Randomly initialize $\hat{\lambda}$

while $optim$ tolerance not met **do**

Reset gradients of $optim$

$\mathbf{X}_{DNN} = DNN(t)$

Compute $\mathbf{X}_{NM} = \text{ODESolve}(t, \mathbf{f}(t; \hat{\lambda}))$

Compute initial condition loss: $\mathcal{L}_{ic}(\theta) = \frac{1}{N_{ic}} \|\mathbf{X}_{DNN}(t_0; \theta) - \mathbf{X}_0(t_0)\|_2^2$

Compute physics loss: $\mathcal{L}_p(\theta) = \frac{1}{N_p} \|\mathbf{X}_{DNN}(t; \theta) - \mathbf{X}_{NM}(t; \hat{\lambda})\|_2^2$

$\mathcal{L}(\theta) = \mathcal{L}_{ic}(\theta) + \mathcal{L}_p(\theta)$

Compute gradients of $\mathcal{L}(\theta)$ using backpropagation

Update θ by taking an $optim$ step

end while

estimating the physical parameters by initializing the neural network parameters θ such that the neural network structure implicitly incorporates the governing equations. This makes the training process more efficient and robust. In fact, as shown in Section 3.1.2, we observe a performance degradation by training the neural network directly without pre-training on the numerical approximation. We use the following terms in (2.7) for pre-training:

$$\mathcal{L}_{ic}(\theta) = \frac{1}{N_{ic}} \|\mathbf{X}_{DNN}(t_0; \theta) - \mathbf{X}_0(t_0)\|_2^2 \quad (2.8)$$

$$\mathcal{L}_p(\theta) = \frac{1}{N_p} \|\mathbf{X}_{DNN}(t; \theta) - \mathbf{X}_{NM}(t; \hat{\lambda})\|_2^2 \quad (2.9)$$

and $\mathcal{L}_d(\theta) = \mathcal{L}_{\lambda_i} = 0$ for all $i = 1, \dots, |\lambda|$. As opposed to the physics loss in (2.4) from Section 2.1, which encodes the known physics given by the observed data, (2.9) in this pre-training phase encodes the known functional form of the RHS given by the numerical solution \mathbf{X}_{NM} . Algorithm 2 provides pseudocode for the neural network pre-training. With each epoch of training, the approximation for the states improve as the neural network parameters update during backpropagation. However, since this step uses randomly initialized physical parameters, the resulting approximation is far from exact, and we require fine-tuning to improve \mathbf{X}_{DNN} further.

2.2.2 Fine-tuning Phase

In the fine-tuning phase of training the neural network, we use the observed data from the system to fine-tune the neural network parameters θ taken from the pre-trained network. We augment the physical parameters $\hat{\lambda}$ to the neural network parameters θ and treat them as trainable parameters $\tilde{\theta} = (\theta, \hat{\lambda})^T$ in the fine-tuning neural network. When using backpropagation and the optimization algorithms to train the neural network, the physical parameters are also updated at each epoch. Thus, we fine-tune the neural network by updating $\tilde{\theta}$ using

Algorithm 3 Neural network fine-tuning to estimate unknown physical parameters

Input: Discretized time steps t , initial conditions \mathbf{X}_0 , randomly initialized physical parameters $\hat{\lambda}$, pre-trained neural network parameters θ

Output: State approximation \mathbf{X}_{DNN} at time steps t , estimated physical parameters $\hat{\lambda}$

Define an optimizer *optim*

Set $\tilde{\theta} = [\theta; \hat{\lambda}]$

while *optim* tolerance not met **do**

 Reset gradients of *optim*

$\mathbf{X}_{DNN} = DNN(t; \tilde{\theta})$

 Compute required gradients of \mathbf{X}_{DNN}

 Compute initial condition loss: $\mathcal{L}_{ic}(\tilde{\theta}) = \frac{1}{N_{ic}} \|\mathbf{X}_{DNN}(t_0; \tilde{\theta}) - \mathbf{X}_0(t_0)\|_2^2$

 Compute physics loss: $\mathcal{L}_p(\tilde{\theta}) = \frac{1}{N_p} \|\hat{\mathbf{f}}_{DNN}(t; \tilde{\theta}) - \mathbf{f}_{param}(t; \hat{\lambda})\|_2^2$

 Compute data loss: $\mathcal{L}_d(\tilde{\theta}) = \frac{1}{N_d} \|\mathbf{X}_{DNN}(t; \tilde{\theta}) - \mathbf{X}_{obs}(t)\|_2^2$

 Compute parameter loss $\forall \lambda_i$: $\mathcal{L}_{\lambda_i} = \min(0, \hat{\lambda}_i - \lambda_i^{min})^2 - \max(0, \hat{\lambda}_i - \lambda_i^{max})^2$

$\mathcal{L}(\tilde{\theta}) = \mathcal{L}_{ic}(\tilde{\theta}) + \mathcal{L}_p(\tilde{\theta}) + \mathcal{L}_d(\tilde{\theta}) + \sum_{i=1}^{|\lambda|} \mathcal{L}_{\lambda_i}$

 Compute gradients of $\mathcal{L}(\tilde{\theta})$ using backpropagation

 Update $\tilde{\theta}$ by taking an *optim* step

end while

observed data and learning the approximated physical parameters $\hat{\lambda}$ in the process. From (2.7), we use the following loss terms to fine-tune the neural network:

$$\mathcal{L}_{ic}(\tilde{\theta}) = \frac{1}{N_{ic}} \|\mathbf{X}_{DNN}(t_0; \tilde{\theta}) - \mathbf{X}_0(t_0)\|_2^2 \quad (2.10)$$

$$\mathcal{L}_p(\tilde{\theta}) = \frac{1}{N_p} \|\hat{\mathbf{f}}_{DNN}(t; \tilde{\theta}) - \mathbf{f}_{param}(t; \hat{\lambda})\|_2^2 \quad (2.11)$$

$$\mathcal{L}_d(\tilde{\theta}) = \frac{1}{N_d} \|\mathbf{X}_{DNN}(t; \tilde{\theta}) - \mathbf{X}_{obs}(t)\|_2^2 \quad (2.12)$$

$$\mathcal{L}_{\lambda_i} = \min(0, \hat{\lambda}_i - \lambda_i^{min})^2 - \max(0, \hat{\lambda}_i - \lambda_i^{max})^2 \quad (2.13)$$

Similar to the physics loss term in (2.4) from Section 2.1, (2.11) in this fine-tuning phase encodes the known physics in the problem, denoted \mathbf{f}_{param} , which is computed using the known functional form of the RHS and estimated physical parameter values, instead of using the observed data directly. The form of the parameter loss terms in (2.13) penalizes estimates for each parameter outside of the range $\hat{\lambda}_i \in [\lambda_i^{min}, \lambda_i^{max}]$, $i = 1, \dots, |\lambda|$. We then sum the individual parameter losses in (2.7). We also remark that the numerical method approximation \mathbf{X}_{NM} is not explicitly used in the loss term for the fine-tuning phase, but due to pre-training the neural network, the numerical approximation implicitly contributes to the learning of $\tilde{\theta}$. Algorithm 3 provides pseudocode for the neural network fine-tuning phase. In the same way as Section 2.1, we refer to the result of the neural network as the model prediction for this problem.

3 Numerical Results

We apply the methods described in Section 2 to a suite of test problems with oscillatory and chaotic dynamics. We use Python3 and PyTorch [60] to construct and train the neural network architectures described in this section. Results were produced locally using an Acer Aspire A515-57 laptop computer with 16 GB RAM and an Intel[®] Core[™] i7-1255U processor. To generate noisy simulated data for our numerical examples, we assume that the observed states are corrupted by Gaussian noise with mean zero and covariance matrix prescribed based on a percentage of the standard deviations of the exact solution trajectories. More specifically, for some discrete times t_j , $j = 1, \dots, T$, we let

$$\mathbf{X}_{obs}(t_j) = \mathbf{X}_{exact}(t_j) + \delta \cdot \boldsymbol{\eta}_j, \quad \boldsymbol{\eta}_j \sim \mathcal{N}(\mathbf{0}, \Gamma) \quad (3.1)$$

where δ represents a user-defined noise level, Γ is an $n \times n$ diagonal matrix with the variance of each state along the main diagonal, and $\mathcal{N}(\cdot, \cdot)$ denotes the multivariate normal distribution.

To evaluate the performance of our models, we pass randomized time steps into the neural network to evaluate the performance of the approximated dynamics and states on data within the domain that the neural network was not trained on. As an evaluation metric, we compute the mean squared error (MSE) between the exact solution and neural network approximation for each state at the test data points:

$$\text{MSE} = \frac{1}{N} \sum_{i=1}^N (y_i - \hat{y}_i)^2 \quad (3.2)$$

where y_i is the true value of the i -th sample, \hat{y}_i is the corresponding predicted value, and N is the number of samples in the test data set. For the method described in Section 2.2, we also compare the estimated physical parameter values with the ground truth values used in generating the data by calculating the relative error. For all the examples in this section, since we are using simulated data and the underlying true dynamics and states are known, we compute the MSE and relative errors using the exact solutions and parameter values compared with their deep learning approximations. However, we acknowledge that in cases where the dynamics of a system are truly unknown, the evaluation of the model becomes more difficult and different metrics are required.

We compare various numerical schemes for computing the state approximations in each method, employing both RK and LMMs within the neural network. In particular, we utilize the explicit Runge–Kutta–Fehlberg method of order 4(5), denoted RK45, for computational efficiency and consider methods from the three main LMM families: Adams-Bashforth (AB), Adams-Moulton (AM), and the backwards differentiation formulae (BDF). In this work, we denote a specific LMM scheme using its family name and number of steps; e.g., AB2 is the 2-step Adams-Bashforth method. Note that while the AB methods are explicit, both the AM and BDF families are implicit and require the solution of an additional optimization problem at each time step. When choosing a numerical ODE solver, the size and shape of the absolute stability regions are critical because they determine which values of the time step will give bounded solutions. In this section, we show results for a suitable choice of numerical method (i.e., one that is stable and well-suited for the problem at hand). We

note that 2-step methods provide a reasonable balance between computational efficiency and accurate results for the examples considered in this work. The supplementary materials include an example comparing performance across different LMM schemes.

3.1 Example 1: FitzHugh-Nagumo

The FitzHugh-Nagumo model is a simplified version of the Hodgkin-Huxley model describing neural spike generation and propagation [61–63]. The behavior is modeled with a short spike of membrane voltage, $v(t)$, which is diminished over time by a slower recovery variable, $w(t)$. The standard form of the governing equations for this dynamical system is

$$\frac{dv}{dt} = v - \frac{v^3}{3} - w + z \quad (3.3)$$

$$\frac{dw}{dt} = \frac{1}{c}(v + a - bw) \quad (3.4)$$

where a , b , and c are system parameters and z corresponds to an applied membrane current. We set $a = 0.7$, $b = 0.8$, $c = 12.5$, and $z = 1$ as the true parameter values and take $v(0) = -2.8$ and $w(0) = -1.8$ as the initial conditions. We consider the solution obtained by using RK45 with a time step of $\Delta t = 0.0001$ as the exact solution for this example.

3.1.1 Dynamics Discovery

We implement a feed-forward neural network with 4 hidden layers and 64 nodes per layer. For both the RK45 and BDF2 schemes, we use the same time step of $\Delta t = 0.1$. Figure 2 shows the resulting FitzHugh-Nagumo model predictions obtained from the neural network trained on observed data with various noise levels and using the RK and LMM schemes, and Table 2 displays the corresponding MSEs between the predictions and exact solutions.

In the case of noiseless data, we see that the model predictions of both $v(t)$ and $w(t)$ very closely match the true states for both numerical schemes. When the noise level increases, more error accrues in the predictions for $v(t)$, whereas the predictions for $w(t)$ remain consistently close to the ground truth. We attribute these results to the larger magnitude of change in the $v(t)$ signal, which corresponds to more noise in the corrupted observations. However, even though the model predictions for $v(t)$ appear more erratic, they remain consistent between the RK and LMM schemes. In fact, Table 2 indicates that the MSEs comparing the model prediction with the exact solution are on the same order of magnitude for both the RK and LMM schemes for each system component and noise level.

3.1.2 Parameter Estimation

For this example, we aim to estimate the unknown physical parameters $\lambda = (a, b, c, z)^T$ in (3.3) and (3.4) given both noiseless and 20% noisy observed data. We use the same time step and neural network architecture as in Section 3.1.1 but concatenate the physical parameter estimates to the pre-trained neural network parameters. Table 1 displays the resulting physical parameter estimates and relative errors for each parameter using both RK45 and AB2 methods. Figure 3 presents the resulting FitzHugh-Nagumo state predictions

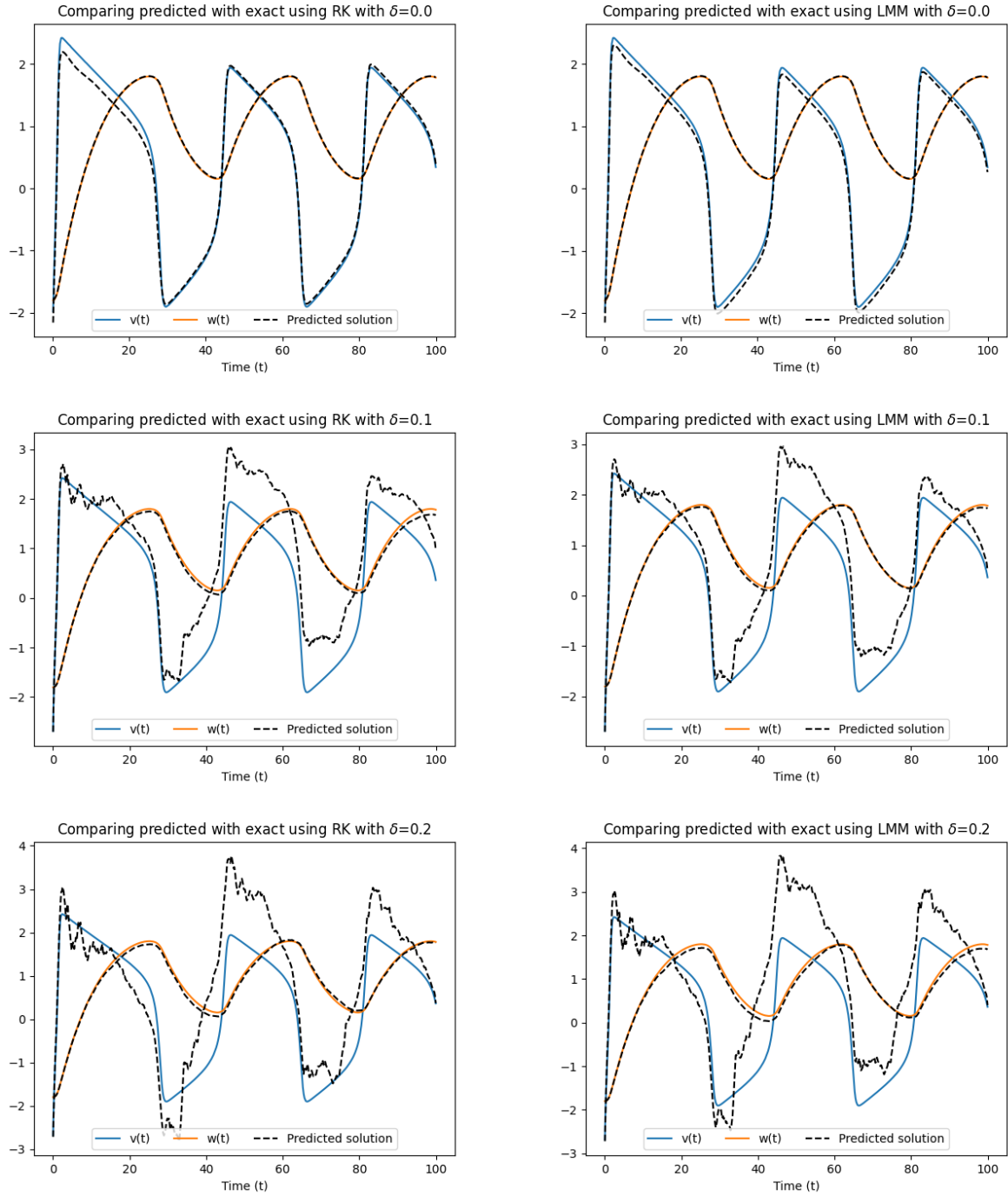


Figure 2: Dynamics discovery model predictions of the FitzHugh-Nagumo model obtained using observed data at various noise levels ($\delta = 0, 0.1, 0.2$) with RK45 and BDF2.

with RK45 computed in two ways: Figure 3a shows the model prediction of $v(t)$ and $w(t)$ using the output of the trained neural network, while Figure 3b displays the state prediction obtained by plugging in the estimated physical parameter values from Table 1 into (3.3) and (3.4) and solving numerically. Table 2 reports the corresponding MSEs computed using the

model predictions and the exact solution described in Section 3.1.

From these results, we observe model predictions close to exact using the neural network output in Figure 3a, which is reflected in the low MSE values in Table 2. Alternatively, the state predictions in Figure 3b using the estimated physical parameter values appear slightly out of phase with the ground truth. We note that several of the estimated physical parameter values have somewhat high relative errors reported in Table 1 compared with the true values used in generating the data. This arises from the fact that we approximate the unknown physical parameters along with the neural network parameters during training. Thus, we observe a compensation for errors in the physical parameter estimates in the estimated neural network parameters θ . To avoid redundancy, Figure 3 displays results using only RK45 as the numerical scheme, but experiments using AB2 provide similar results.

As detailed in Section 2.2, the method for physical parameter estimation utilizes a pre-training step to initialize the neural network parameters θ before fine-tuning the neural network for estimating physical parameter values. Without this additional step, the task of approximating system states and physical parameters becomes much more difficult and the resulting predictions are not as accurate. To highlight the importance of this pre-training phase, Figure 4 and Table 3 display the results of applying the same neural network architecture described above but removing the pre-training step. That is, we only use the fine-tuning training described in Section 2.2.2 with the augmented parameter vector $\tilde{\theta} = (\theta; \hat{\lambda})^T$, where the neural network parameters θ are randomly initialized instead of coming from pre-training. As seen in Figure 4, the predicted solutions for $v(t)$ and $w(t)$ are nowhere near as close to the exact solutions with 20% noisy data, losing the dynamics in both components around time $t \in (10, 20)$, which is also reflected in the relatively high MSEs compared to the results that included the pre-training step (see Table 2). When comparing the physical parameter estimates, several of the estimated values obtained without pre-training in Table 3 do not update from their initial values, similar to the case with pre-training. We note that while the relative errors for some parameter estimates are smaller compared to the corresponding results with pre-training (see Table 1), the pre-trained neural network parameters allow the network to better learn the system dynamics via the numerical solution of the system, resulting in better model predictions than without pre-training.

3.2 Example 2: Lorenz-63 System

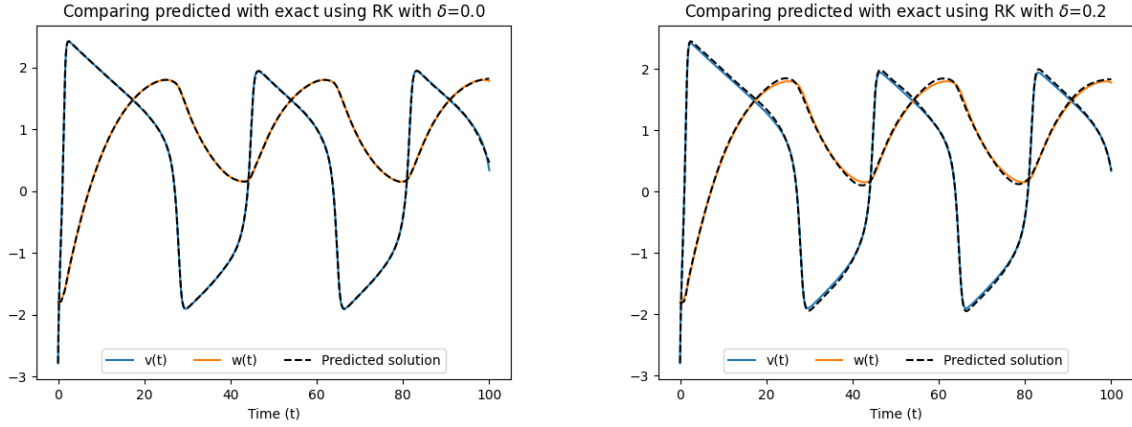
The Lorenz-63 system provides a model of atmospheric convection that is notable for its chaotic solutions for certain choices of initial conditions and parameters [64]. The governing equations are of the form

$$\frac{dx}{dt} = \sigma(y - x) \tag{3.5}$$

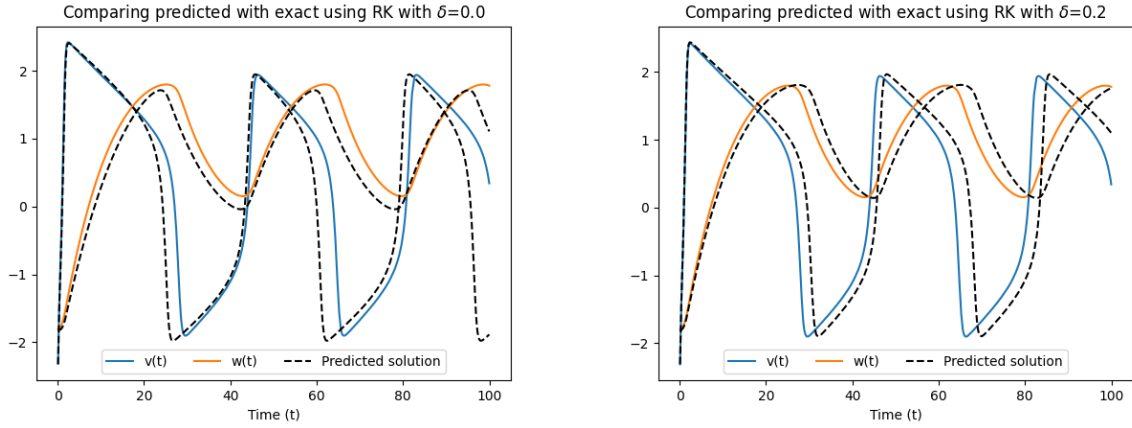
$$\frac{dy}{dt} = x(\rho - z) - y \tag{3.6}$$

$$\frac{dz}{dt} = xy - \beta z \tag{3.7}$$

where the parameters $\sigma = 10$, $\beta = 8/3$, and $\rho = 28$ are chosen such that the system exhibits chaotic behavior. In addition to these parameter values, we set the initial conditions



(a) Model predictions of the states $v(t)$ and $w(t)$ using the output of the trained neural network.



(b) State predictions computed from RK45 using estimated parameter values in Table 1.

Figure 3: Parameter estimation predictions of the FitzHugh-Nagumo model states obtained using observed data at various noise levels ($\delta = 0, 0.2$) with RK45.

$x(0) = -8$, $y(0) = 7$, and $z(0) = 27$ to apply our method for this example. We approximate the exact solution of the Lorenz-63 system using RK45 at a fine time step of $\Delta t = 0.00025$.

3.2.1 Dynamics Discovery

As in Section 3.1.1, we apply the method of discovering unknown system dynamics using observed data with noise levels of 0%, 10%, and 20%. We include results using noiseless observed data to distinguish predictions due to chaos versus results due to noise in the training data. When training on noiseless data, we implement a feed-forward neural network with 4 hidden layers and 64 nodes per layer with a skip connection, which bypasses the hidden layers and adds back an identity function to the output node [65]. This provides an alternate path for the gradient in backpropagation and reduces model overfitting, particularly for this chaotic problem. To reduce overfitting on substantially noisy data, we choose a less complex neural network architecture of 32 hidden nodes in 1 layer with a skip connection. For both

	Parameter	True Value	Noise Level	Initial Value	Estimate	Relative Error
RK	a	0.7	0%	0.386	0.507	0.276
			20%	0.418	0.545	0.222
	b	0.8	0%	0.417	0.505	0.369
			20%	0.091	0.722	0.097
	c	12.5	0%	14.175	12.926	0.034
			20%	13.084	12.955	0.036
	z	1	0%	0.572	0.814	0.186
			20%	1.021	1.021	0.021
LMM	a	0.7	0%	0.510	0.510	0.272
			20%	0.003	0.652	0.068
	b	0.8	0%	0.625	0.625	0.219
			20%	0.636	0.636	0.205
	c	12.5	0%	13.667	12.897	0.032
			20%	13.636	12.940	0.035
	z	1	0%	0.876	0.876	0.124
			20%	0.567	0.871	0.129

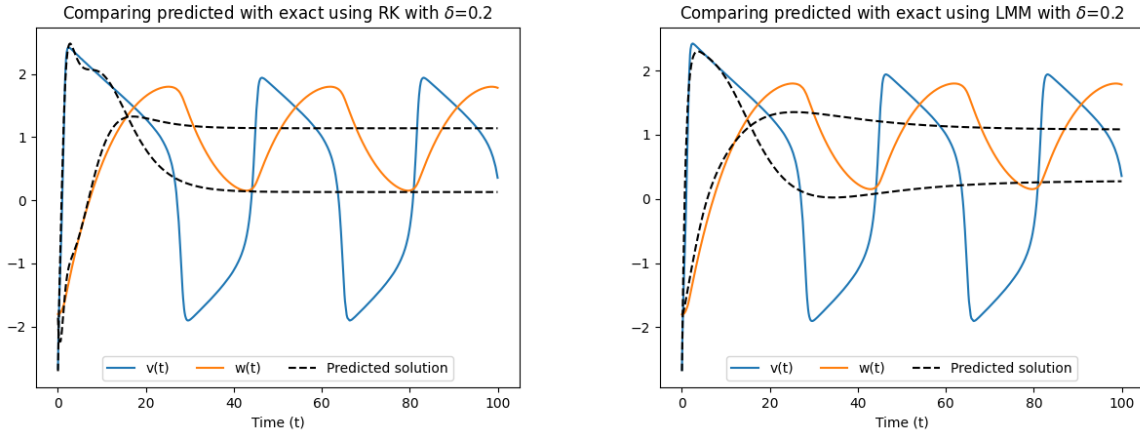
Table 1: Estimated physical parameter values from the FitzHugh-Nagumo model obtained using noiseless and 20% noisy observed data with RK (RK45) and LMM (AB2) schemes. Initial values (from pre-training), estimated values, and relative errors are reported to three decimal places.

	Noise Level	RK		LMM	
		v	w	v	w
Dynamics Discovery	0%	1.34e-02	8.28e-05	1.02e-02	7.00e-05
	10%	5.02e-01	5.05e-04	3.02e-01	3.20e-04
	20%	7.50e-01	3.95e-03	1.66e-01	4.47e-03
Parameter Estimation	0%	9.50e-05	3.21e-05	2.45e-04	3.12e-05
	20%	2.49e-03	1.67e-03	2.98e-03	1.81e-03

Table 2: Comparing RK and LMM scheme MSEs for FitzHugh-Nagumo model predictions. For this example, we use BDF2 for dynamics discovery and AB2 for parameter estimation as our LMMs.

the RK45 and BDF2 schemes, we use a time step of $\Delta t = 0.001$. Figure 5 displays the predicted states of the Lorenz-63 system using the LMM scheme, and Table 5 presents the corresponding MSEs for both RK45 and BDF2.

For the noiseless case, the dynamics of the $x(t)$ component are fairly well recovered, but the predictions for $y(t)$ and $z(t)$ begin to drift away from the exact solutions. This “drifting” results from error propagation within the neural network. Due to the inherent chaos and instability of the Lorenz-63 system, errors grow significantly. This challenge is further exacerbated by the complexity of the dynamics discovery problem in the presence of noise. As the noise level increases, we observe more drifting in the state predictions, particularly in the $y(t)$ and $z(t)$ components. However, the MSEs in Table 5 are again on the same order of magnitude for both the RK and LMM schemes for each system component



(a) MSE for states $v(t)$ and $w(t)$ are $1.51e+00$ and $3.17e-01$, respectively. (b) MSE for states $v(t)$ and $w(t)$ are $1.48+00$ and $2.95e-01$, respectively.

Figure 4: Parameter estimation model predictions of FitzHugh-Nagumo model with 20% noisy data for RK (RK45) and LMM (AB2) schemes without pre-training.

	Parameter	True Value	Initial Value	Estimated Value	Relative Error
RK	a	0.7	0.252	0.585	0.165
	b	0.8	0.083	0.642	0.197
	c	12.5	10.048	12.405	0.008
	z	1	1.147	1.147	0.147
LMM	a	0.7	0.981	0.853	0.218
	b	0.8	0.566	0.566	0.293
	c	12.5	11.181	12.435	0.005
	z	1	1.018	1.018	0.018

Table 3: Estimated physical parameter values from the FitzHugh-Nagumo model obtained using 20% noisy observed data with RK (RK45) and LMM (AB2) schemes without pre-training. Randomly initialized values, estimated values, and relative errors are reported to three decimal places.

and noise level, indicating reasonable predictions in the presence of corrupted data.

3.2.2 Parameter Estimation

For this problem, we aim to estimate the physical parameter values $\lambda = (\sigma, \beta, \rho)^T$ from (3.5), (3.6), and (3.7) given both noiseless and noisy observed data. We implement a feed-forward neural network with 4 hidden layers and 64 nodes per layer with a skip connection and use the same time step as in Section 3.2.1. Table 4 displays the estimated parameter values from the neural network training on noiseless and 20% noisy data using RK45 and AB2, and Figure 6 shows the model predictions of $x(t)$, $y(t)$, and $z(t)$ with AB2.

Results show close model predictions at certain time points but also large deviations due to the unstable solution in both the noiseless and noisy cases. The predictions shown in

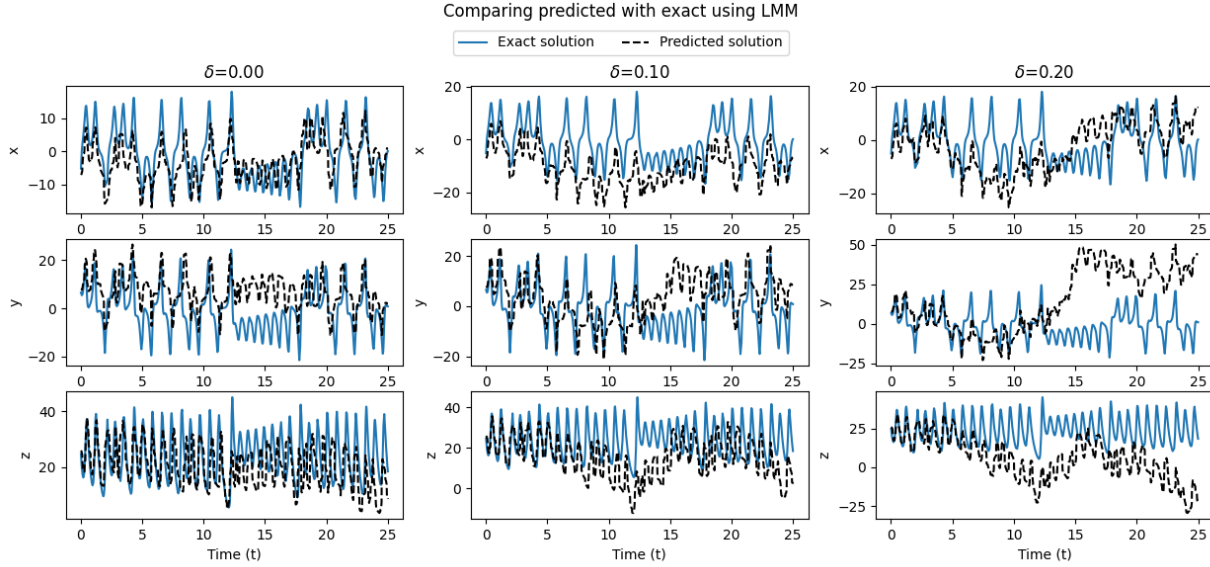


Figure 5: Dynamics discovery model predictions of the Lorenz-63 system obtained using noisy observed data at various noise levels ($\delta = 0, 0.1, 0.2$) with BDF2.

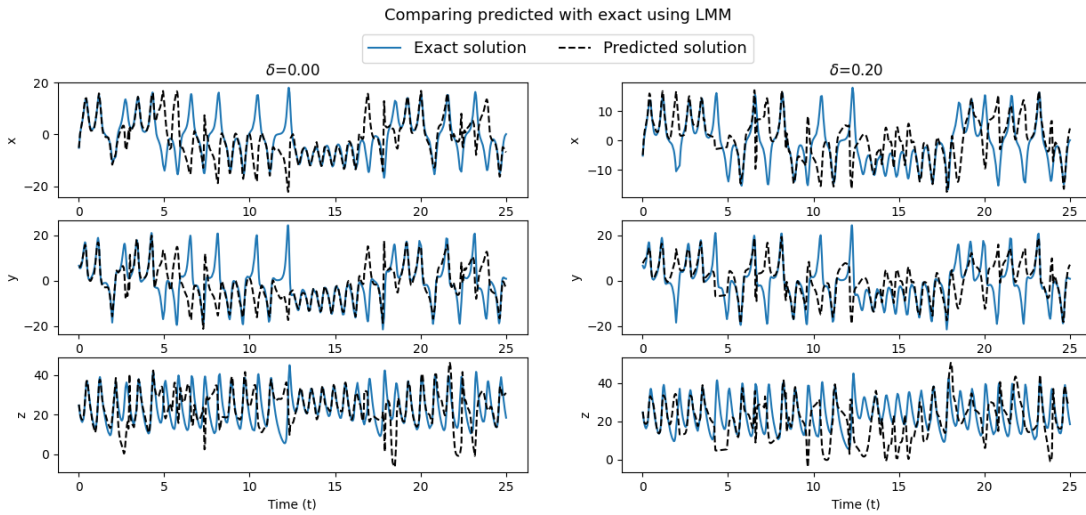


Figure 6: Parameter estimation model predictions of the Lorenz-63 system obtained using the output of the neural network trained on noiseless and 20% noisy data with AB2.

Figure 6 appear to lose significant accuracy in capturing the system dynamics, particularly in $z(t)$, but this is also observed in the dynamics discovery case and can be attributed to the chaotic nature of the system. This is further reflected in the relatively high MSE values in Table 5 compared to the other examples, but the orders of the MSEs are comparable to the other Lorenz-63 examples. Despite errors in the model predictions, the physical parameter values in Table 4 are fairly well recovered, especially in the case of noisy data, with relative errors mostly on the order of 10^{-2} . We also observe similar levels of accuracy between RK and LMM methods in both the model predictions and physical parameter estimates.

	Parameter	True Value	Noise Level	Initial Value	Estimate	Relative Error
RK	σ	10	0%	9.238	9.528	0.047
			20%	8.732	9.089	0.091
	β	2.667	0%	2.355	2.462	0.077
			20%	3.211	3.014	0.130
	ρ	28	0%	27.318	27.444	0.020
			20%	25.962	26.455	0.055
LMM	σ	10	0%	11.830	11.691	0.169
			20%	10.078	10.078	0.008
	β	2.667	0%	3.129	3.055	0.146
			20%	2.857	2.749	0.031
	ρ	28	0%	26.694	26.787	0.043
			20%	28.921	28.704	0.025

Table 4: Estimated physical parameter values from the Lorenz-63 model obtained using noiseless and 20% noisy observed data with RK (RK45) and LMM (AB2) schemes. Initial values (from pre-training), estimates, and relative errors are reported to three decimal places.

	Noise Level	RK			LMM		
		x	y	z	x	y	z
Dynamics Discovery	0%	4.55e+01	1.25e+02	1.32e+02	4.51e+01	1.35e+02	1.06e+02
	10%	1.31e+02	1.68e+02	2.02e+02	1.29e+02	1.25e+02	2.06e+02
	20%	1.11e+02	6.93e+02	4.61e+02	9.42e+01	6.81e+02	5.64e+02
Parameter Estimation	0%	9.36e+01	9.83e+01	1.65e+02	8.12e+01	8.12e+01	1.13e+02
	20%	1.00e+02	1.18e+02	1.56e+02	8.07e+01	9.27e+01	1.72e+02

Table 5: Comparing RK and LMM scheme MSEs for Lorenz-63 system model predictions. For this example, we use BDF2 for dynamics discovery and AB2 for parameter estimation as our LMMs.

3.3 Example 3: Heat Equation

The heat equation is a PDE that models how heat diffuses through a spatial region; see, e.g., [66]. We consider the one-dimensional heat equation, modeling the change in temperature over time as

$$\frac{\partial u}{\partial t} = k \frac{\partial^2 u}{\partial x^2}, \quad 0 \leq x \leq L, \quad t \geq 0 \quad (3.8)$$

with constant diffusion coefficient k and the following initial and Robin boundary conditions:

$$u(x, 0) = \sin\left(\frac{\pi x}{2}\right), \quad (3.9)$$

$$u(0, t) = 0, \quad (3.10)$$

$$\frac{\partial u}{\partial x}(L, t) = 0. \quad (3.11)$$

The analytic solution to this problem using separation of variables and Fourier series is

$$u(x, t) = \sin\left(\frac{\pi x}{2}\right) \exp\left(-\frac{\pi^2 t}{4}\right). \quad (3.12)$$

For this example, we assume that $k = 1$, $L = 1$, and $t \in [0, 2.5]$.

3.3.1 Method of Lines Approximation

The method of lines (MOL) approach for numerically solving PDEs discretizes the spatial dimension first, resulting in a system of coupled ODEs where each component corresponds to the solution at some spatial grid point as a function of time [67]. We then compute the approximate solution of the ODE system using a numerical method such as RK or LMM. Discretizing the spatial variable into $M + 1$ points, we replace the spatial derivative in (3.8) using the second-order central difference formula:

$$\frac{\partial^2 u}{\partial x^2} \approx D_0^2 u = \frac{u_{i+1} - 2u_i + u_{i-1}}{h^2} \quad (3.13)$$

where $u_i = u_i(t) \approx u(x_i, t)$ and $h = \Delta x$ denotes the spatial step size, with approximation error $\mathcal{O}(h^2)$. This discretization leads to the following MOL approximation of (3.8):

$$\frac{du_i}{dt} = k \frac{u_{i+1} - 2u_i + u_{i-1}}{h^2}, \quad 1 \leq i \leq M - 1. \quad (3.14)$$

Spatial discretization of the initial and boundary conditions yields

$$u_i(0) = \sin\left(\frac{\pi x_i}{2}\right), \quad 0 \leq i \leq M, \quad (3.15)$$

$$u_0(t) = 0, \quad t \geq 0, \quad (3.16)$$

$$\frac{u_M(t) - u_{M-1}(t)}{h} = 0, \quad t \geq 0, \quad (3.17)$$

using a forward difference approximation for (3.11), which implies that $u_M(t) = u_{M-1}(t)$.

3.3.2 Dynamics Discovery

For dynamics discovery, we implement a neural network architecture with the 64 hidden nodes per layer and 2 hidden layers. For both numerical schemes, we discretize the spatial variable into $M + 1$ equispaced points where $M = 20$ and use a time step of $\Delta t = 0.00227$ to account for stability of the numerical methods. Figure 7 shows the heat equation model predictions at spatial location $x = 0.5$ with 20% noisy data for both RK45 and BDF2 schemes. These results are similar to the previous two examples, given appropriate choices for the spatial and temporal discretizations. We observe close predictions to the ground truth at $x = 0.5$ and correspondingly small MSEs in Table 6. While not shown, results at different spatial locations are similar to those at $x = 0.5$.

3.3.3 Parameter Estimation

For parameter estimation, we use the same spatial discretization and the same feed-forward neural network as in Section 3.3.2 but with a skip connection as in Section 3.2.2. We take $\Delta t = 0.02$ as the time step for this example. Figure 8 shows the predicted temperature at $x = 0.5$ using the estimated parameters with RK45 and BDF2. As in the dynamics discovery

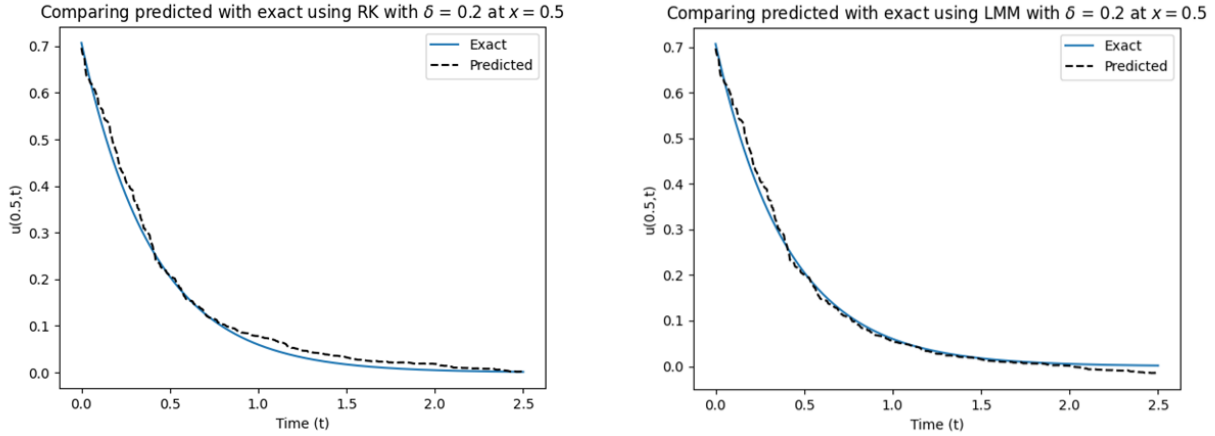
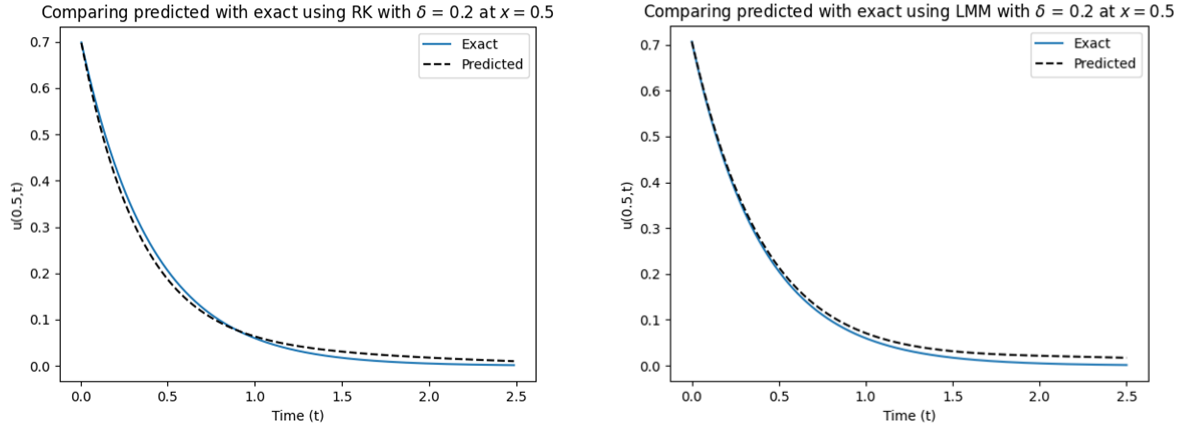


Figure 7: Dynamics discovery model predictions of the heat equation at spatial location $x = 0.5$ obtained using 20% noisy data with RK45 and BDF2.



(a) Initial value of $k \approx 1.470$,
Estimated value of $k \approx 1.415$.

(b) Initial value of $k \approx 1.376$,
Estimated value of $k \approx 1.320$.

Figure 8: Parameter estimation model predictions of the heat equation at spatial location $x = 0.5$ obtained using the output of the neural network trained on 20% noisy data with RK45 and BDF2.

examples, the model predictions in Figure 8 are reasonably accurate, with correspondingly low MSEs in Table 6 and similar results across methods. While the relative errors in the final parameter estimates of the diffusion coefficient k are somewhat high (0.415 for RK45 and 0.320 for BDF2, respectively), this error is offset by the estimated neural network parameters, allowing the model predictions to remain fairly accurate.

	Noise Level	RK	LMM
Dynamics Discovery	10%	3.03e-03	1.74e-03
	20%	2.86e-03	2.78e-03
Parameter Estimation	20%	6.80e-04	6.29e-04

Table 6: Comparing RK and LMM scheme MSE for the heat equation model predictions. For this example, we use BDF2 as the LMM for both problems of interest.

4 Discussion and Conclusions

This work presents two novel approaches combining deep learning and numerical methods to address dynamics discovery and parameter estimation in deterministic dynamical systems. In problems where physics is missing, we augment neural network training with numerical ODE solvers to approximate unknown system states and physical parameters. Implementing the proposed methods on a suite of test problems provides empirical evidence that combining a constrained neural network with numerical methods such as RK45 and LMMs leads to promising predictions of unknown system dynamics and physical parameters, even with significant Gaussian noise corrupting the observed data. Our models demonstrate strong generalization when applied to oscillatory and chaotic problems.

Results using RK and LMM families of methods are comparable, given appropriate choices of time step, order, and neural network architecture. As illustrated in Section 3, the choice of implicit LMMs such as BDF results in good predictions, but these methods require solving a nonlinear optimization problem at every step in addition to the non-convex optimization problem when training the neural network. From Tables 2, 5 and 6, we observe similar MSE values between RK and LMM when comparing the model prediction with the exact solutions, computed either numerically using RK45 at very fine time steps (as in Sections 3.1 and 3.2) or analytically (as in Section 3.3).

We did not observe significant differences in the resulting predictions and parameter estimates due to the addition of noise in the observed data, suggesting that our proposed approaches are robust to noise. However, the test examples used noisy data generated from known solutions since we considered well-known problems in computational science. In future work, we will apply these methods to real-world datasets that contain significant noise (as well as modeling errors) and are more representative of missing physics in dynamical systems. Moreover, we will investigate methods to account for this noise, not only within the testing data but also the neural network itself. We will explore techniques for modeling uncertainty and noise within the proposed architecture.

When estimating the system physical parameters, we observe that the proposed method implementing a pre-training and fine-tuning phase recovers values reasonably close to the exact, even when trained on data perturbed with significant Gaussian noise. Moreover, the method provides accurate predictions of the system states using the estimated parameters $\hat{\lambda}$, even when the parameters include some approximation errors, as demonstrated with the low MSEs in Tables 2, 5 and 6. In some cases, the final physical parameter estimates include relatively large approximation errors or remain unchanged during the neural network training for both the noiseless and noisy cases. This arises from the fact that the unknown physical parameters are optimized along with the neural network parameters. When training the

neural network, the prediction improves because of the tuned neural network parameters θ even though the learned physical parameters $\hat{\lambda}$ may differ from their exact values. Physical parameters that do not update may be unidentifiable from the given data or randomly initialized to reasonable approximations already in the pre-training phase.

To address the problem of overfitting, we chose less complex neural network architectures and added skip connections to improve training. However, we acknowledge that because the loss functions in Section 2 include an initial condition loss term, i.e., the terms in (2.3), (2.8), and (2.10), the predicted solutions are biased to match the input data at time $t = 0$. Thus, when using testing data generated from different initial conditions, the predictions will remain consistent with solutions from the initial conditions the neural network was trained on. In future work, we will consider ways to improve the training such that the resulting models can generalize more readily to testing data with different initial conditions. Further, in combining neural networks and numerical ODE solvers, we note that the choice of hyperparameters involving the spatial and temporal discretization schemes, numerical method orders, and neural network architectures play a significant role in our proposed method, with appropriate choices of these settings leading to promising results. We will further investigate what constitutes a good choice of these hyperparameters and how to choose them optimally in future work.

Data Availability Statement: Code and data that reproduce the results in this paper are available upon reasonable request.

Declaration of Competing Interest: None.

References

- [1] S. L. Brunton, J. L. Proctor, and J. N. Kutz. Discovering governing equations from data by sparse identification of nonlinear dynamical systems. *Proceedings of the National Academy of Sciences*, 113(15):3932–3937, 2016.
- [2] S. H. Rudy, J. N. Kutz, and S. L. Brunton. Deep learning of dynamics and signal-noise decomposition with time-stepping constraints. *Journal of Computational Physics*, 396:483–506, 2019.
- [3] M. Raissi. Deep hidden physics models: Deep learning of nonlinear partial differential equations. *J. Mach. Learn. Res.*, 19(1):932–955, 2018.
- [4] M. Raissi, P. Perdikaris, and G. E. Karniadakis. Multistep neural networks for data-driven discovery of nonlinear dynamical systems. *arXiv.org [Preprint]*, 2018. <https://arxiv.org/abs/1801.01236>.
- [5] R. Tipireddy, P. Perdikaris, P. Stinis, and A. M. Tartakovsky. Multistep and continuous physics-informed neural network methods for learning governing equations and constitutive relations. *Journal of Machine Learning for Modeling and Computing*, 3(2):23–46, 2022.

- [6] M. Raissi, P. Perdikaris, and G. E. Karniadakis. Physics-informed neural networks: A deep learning framework for solving forward and inverse problems involving nonlinear partial differential equations. *Journal of Computational Physics*, 378:686–707, 2019.
- [7] L. Lu, P. Jin, G. Pang, Z. Zhang, and G. E. Karniadakis. Learning nonlinear operators via DeepONet based on the universal approximation theorem of operators. *Nature Machine Intelligence*, 3(3):218–229, 2021.
- [8] D. N. Tanyu, J. Ning, T. Freudenberg, N. Heilenkötter, A. Rademacher, U. Iben, and P. Maass. Deep learning methods for partial differential equations and related parameter identification problems. *Inverse Problems*, 39(10):103001, 2023.
- [9] N. Baker, F. Alexander, T. Bremer, A. Hagberg, Y. Kevrekidis, H. Najm, M. Parashar, A. Patra, J. Sethian, S. Wild, K. Willcox, and S. Lee. Workshop report on basic research needs for scientific machine learning: Core technologies for artificial intelligence. Technical report, U. S. Department of Energy Office of Science, Advanced Scientific Computing Research, Washington, DC, USA, 2019.
- [10] G. E. Karniadakis, I. G. Kevrekidis, L. Lu, P. Perdikaris, S. Wang, and L. Yang. Physics-informed machine learning. *Nature Reviews Physics*, 3(6):422–440, 2021.
- [11] S. Cuomo, V. S. Di Cola, F. Giampaolo, G. Rozza, M. Raissi, and F. Piccialli. Scientific machine learning through physics-informed neural networks: Where we are and what’s next. *Journal of Scientific Computing*, 92(3):88, 2022.
- [12] J. Willard, X. Jia, S. Xu, M. Steinbach, and V. Kumar. Integrating scientific knowledge with machine learning for engineering and environmental systems. *ACM Comput. Surv.*, 55(4):1–37, 2022.
- [13] L. Lu, X. Meng, Z. Mao, and G. E. Karniadakis. DeepXDE: A deep learning library for solving differential equations. *SIAM Review*, 63(1):208–228, 2021.
- [14] V. Churchill, Y. Chen, Z. Xu, and D. Xiu. DNN modeling of partial differential equations with incomplete data. *Journal of Computational Physics*, 493:112502, 2023.
- [15] S. Wang, Y. Teng, and P. Perdikaris. Understanding and mitigating gradient flow pathologies in physics-informed neural networks. *SIAM Journal on Scientific Computing*, 43(5):A3055–A3081, 2021.
- [16] A. D. Jagtap, E. Kharazmi, and G. E. Karniadakis. Conservative physics-informed neural networks on discrete domains for conservation laws: Applications to forward and inverse problems. *Computer Methods in Applied Mechanics and Engineering*, 365:113028, 2020.
- [17] A. D. Jagtap and G. E. Karniadakis. Extended physics-informed neural networks (XPINNs): A generalized space-time domain decomposition based deep learning framework for nonlinear partial differential equations. *Communications in Computational Physics*, 28(5):2002–2041, 2020.

- [18] B. Moseley, A. Markham, and T. Nissen-Meyer. Finite basis physics-informed neural networks (FBPINNs): a scalable domain decomposition approach for solving differential equations. *Advances in Computational Mathematics*, 49(4):62, 2023.
- [19] V. Dolean, A. Heinlein, S. Mishra, and B. Moseley. Multilevel domain decomposition-based architectures for physics-informed neural networks. *Computer Methods in Applied Mechanics and Engineering*, 429:117116, 2024.
- [20] K. L. Lim, R. Dutta, and M. Rotaru. Physics informed neural network using finite difference method. In *2022 IEEE International Conference on Systems, Man, and Cybernetics*, pages 1828–1833, 2022.
- [21] P.-H. Chiu, J. C. Wong, C. Ooi, M. H. Dao, and Y.-S. Ong. CAN-PINN: A fast physics-informed neural network based on coupled-automatic-numerical differentiation method. *Computer Methods in Applied Mechanics and Engineering*, 395:114909, 2022.
- [22] S. Markidis. The old and the new: Can physics-informed deep-learning replace traditional linear solvers? *Frontiers in Big Data*, 4:669097, 2021.
- [23] W. Zhai, D. Tao, and Y. Bao. Parameter estimation and modeling of nonlinear dynamical systems based on Runge–Kutta physics-informed neural network. *Nonlinear Dynamics*, 111:21117–21130, 2023.
- [24] Z. Chen, Y. Liu, and H. Sun. Physics-informed learning of governing equations from scarce data. *Nature Communications*, 12(1):6136, 2021.
- [25] R. T. Q. Chen, Y. Rubanova, J. Bettencourt, and D. Duvenaud. Neural ordinary differential equations. In S. Bengio, H. Wallach, H. Larochelle, K. Grauman, N. Cesa-Bianchi, and R. Garnett, editors, *Advances in Neural Information Processing Systems 31 (NeurIPS 2018)*, page 6571–6583, 2018.
- [26] J. Kaipio and E. Somersalo. *Statistical and Computational Inverse Problems*. Springer, New York, 2005.
- [27] F. A. C. Viana and A. K. Subramaniyan. A survey of Bayesian calibration and physics-informed neural networks in scientific modeling. *Archives of Computational Methods in Engineering*, 28(5):3801–3830, 2021.
- [28] A. Tarantola. *Inverse Problem Theory and Methods for Model Parameter Estimation*. Society for Industrial and Applied Mathematics, Philadelphia, 2005.
- [29] M. L. Johnson and L. M. Faunt. Parameter estimation by least-squares methods. *Methods Enzymol*, 210:1–37, 1992.
- [30] H. T. Banks, S. Hu, and W. C. Thompson. *Modeling and Inverse Problems in the Presence of Uncertainty*. CRC Press, New York, 2014.
- [31] H. Haario, M. Laine, A. Mira, and E. Saksman. DRAM: Efficient adaptive MCMC. *Statistics and Computing*, 16:339–354, 2006.

- [32] J. Liu and M. West. Combined parameter and state estimation in simulation-based filtering. In A. Doucet, N. Freitas, and N. Gordon, editors, *Sequential Monte Carlo Methods in Practice*, pages 197–223, New York, 2001. Springer.
- [33] A. Arnold, D. Calvetti, and E. Somersalo. Linear multistep methods, particle filtering and sequential Monte Carlo. *Inverse Problems*, 29(8):085007, 2013.
- [34] G. Evensen. The ensemble Kalman filter for combined state and parameter estimation. *IEEE Control Syst Mag*, 29:83–104, 2009.
- [35] A. Arnold, D. Calvetti, and E. Somersalo. Parameter estimation for stiff deterministic dynamical systems via ensemble Kalman filter. *Inverse Problems*, 30(10):105008, 2014.
- [36] A. Arnold. When artificial parameter evolution gets real: Particle filtering for time-varying parameter estimation in deterministic dynamical systems. *Inverse Problems*, 39(1):014002, 2023.
- [37] T. Gaskin, G. A. Pavliotis, and M. Girolami. Neural parameter calibration for large-scale multiagent models. *Proceedings of the National Academy of Sciences*, 120(7):e2216415120, 2023.
- [38] V. Grimm, A. Heinlein, A. Klawonn, M. Lanser, and J. Weber. Estimating the time-dependent contact rate of SIR and SEIR models in mathematical epidemiology using physics-informed neural networks. *Electron. Trans. Numer. Anal.*, 56:1–27, 2022.
- [39] M. Abadi and G. D. Plotkin. A simple differentiable programming language. *Proc. ACM Program. Lang.*, 4(POPL), 12 2019.
- [40] J. Bezanson, A. Edelman, S. Karpinski, and V. B. Shah. Julia: A fresh approach to numerical computing. *SIAM Review*, 59(1):65–98, 2017.
- [41] R. Frostig, M. J. Johnson, and C. Leary. Compiling machine learning programs via high-level tracing. *Systems for Machine Learning*, 4(9), 2018.
- [42] J. Bradbury, R. Frostig, P. Hawkins, M. J. Johnson, C. Leary, D. Maclaurin, G. Necula, A. Paszke, J. V. Plas, S. Wanderman-Milne, and Q. Zhang. JAX: composable transformations of Python+NumPy programs, 2018. <https://github.com/google/jax>.
- [43] N. Thurey, P. Holl, M. Mueller, P. Schnell, F. Trost, and K. Um. *Physics-based Deep Learning*. WWW, 2022. <https://physicsbaseddeeplearning.org>.
- [44] F. de Avila Belbute-Peres, K. Smith, K. Allen, J. Tenenbaum, and J. Z. Kolter. End-to-end differentiable physics for learning and control. In S. Bengio, H. Wallach, H. Larochelle, K. Grauman, N. Cesa-Bianchi, and R. Garnett, editors, *Advances in Neural Information Processing Systems 31 (NeurIPS 2018)*, pages 7178–7189, 2018.
- [45] B. Ramsundar, D. Krishnamurthy, and V. Viswanathan. Differentiable physics: A position piece. *arXiv.org [Preprint]*, 2021. <https://arxiv.org/abs/2109.07573>.

- [46] C. Rackauckas, Y. Ma, J. Martensen, C. Warner, K. Zubov, R. Supekar, D. Skinner, A. Ramadhan, and A. Edelman. Universal differential equations for scientific machine learning. *arXiv.org [Preprint]*, 2021. <https://arxiv.org/abs/2001.04385>.
- [47] A. G. Baydin, B. A. Pearlmutter, A. A. Radul, and J. M. Siskind. Automatic differentiation in machine learning: A survey. *J. Mach. Learn. Res.*, 18(1):5595–5637, 2017.
- [48] W. Grathwohl, R. T. Q. Chen, J. Bettencourt, and D. Duvenaud. Scalable reversible generative models with free-form continuous dynamics. In *International Conference on Learning Representations*, pages 1–14, 2019.
- [49] T. Zhang, Z. Yao, A. Gholami, J. E. Gonzalez, K. Keutzer, M. W. Mahoney, and G. Biros. ANODEV2: A coupled neural ODE framework. In H. Wallach, H. Larochelle, A. Beygelzimer, F. d'Alché-Buc, E. Fox, and R. Garnett, editors, *Advances in Neural Information Processing Systems 32 (NeurIPS 2019)*, pages 5151–5161, 2019.
- [50] K. M. Choromanski, J. Q. Davis, V. Likhoshesterov, X. Song, J.-J. Slotine, J. Varley, H. Lee, A. Weller, and V. Sindhvani. Ode to an ODE. In H. Larochelle, M. Ranzato, R. Hadsell, M. F. Balcan, and H. Lin, editors, *Advances in Neural Information Processing Systems 33 (NeurIPS 2020)*, pages 3338–3350, 2020.
- [51] P. Kidger, J. Morrill, J. Foster, and T. Lyons. Neural controlled differential equations for irregular time series. In H. Larochelle, M. Ranzato, R. Hadsell, M. F. Balcan, and H. Lin, editors, *Advances in Neural Information Processing Systems 33 (NeurIPS 2020)*, pages 6696–6707, 2020.
- [52] E. De Brouwer, J. Simm, A. Arany, and Y. Moreau. GRU-ODE-Bayes: Continuous modeling of sporadically-observed time series. In H. Wallach, H. Larochelle, A. Beygelzimer, F. d'Alché-Buc, E. Fox, and R. Garnett, editors, *Advances in Neural Information Processing Systems 32 (NeurIPS 2019)*, pages 7379–7390, 2019.
- [53] P. Goyal and P. Benner. Neural ordinary differential equations with irregular and noisy data. *Royal Society Open Science*, 10(7):221475, 2023.
- [54] L. Yang, X. Meng, and G. E. Karniadakis. B-PINNs: Bayesian physics-informed neural networks for forward and inverse PDE problems with noisy data. *Journal of Computational Physics*, 425:109913, 2021.
- [55] P. Pilar and N. Wahlström. Physics-informed neural networks with unknown measurement noise. In Alessandro Abate, Mark Cannon, Kostas Margellos, and Antonis Papachristodoulou, editors, *Proceedings of the 6th Annual Learning for Dynamics & Control Conference*, volume 242 of *Proceedings of Machine Learning Research*, pages 235–247. PMLR, 15–17 Jul 2024.
- [56] J. O’Leary, J. A. Paulson, and A. Mesbah. Stochastic physics-informed neural ordinary differential equations. *Journal of Computational Physics*, 468:111466, 2022.

- [57] L. S. Pontryagin. *Mathematical Theory of Optimal Processes*. Taylor & Francis, 1987.
- [58] D. P. Kingma and J. Ba. Adam: A method for stochastic optimization. *arXiv.org [Preprint]*, 2017. <https://arxiv.org/abs/1412.6980>.
- [59] D. C. Liu and J. Nocedal. On the limited memory BFGS method for large scale optimization. *Mathematical Programming*, 45(1):503–528, 1989.
- [60] A. Paszke, S. Gross, F. Massa, A. Lerer, J. Bradbury, G. Chanan, T. Killeen, Z. Lin, N. Gimelshein, L. Antiga, A. Desmaison, A. Köpf, E. Yang, Z. DeVito, M. Raison, A. Tejani, S. Chilamkurthy, B. Steiner, L. Fang, J. Bai, and S. Chintala. PyTorch: An imperative style, high-performance deep learning library. *arXiv.org [Preprint]*, 2019. <https://arxiv.org/abs/1912.01703>.
- [61] R. FitzHugh. Impulses and physiological states in theoretical models of nerve membrane. *Biophysical Journal*, 1(6):445–466, 1961.
- [62] J. Nagumo, S. Arimoto, and S. Yoshizawa. An active pulse transmission line simulating nerve axon. *Proceedings of the IRE*, 50(10):2061–2070, 1962.
- [63] A. L. Hodgkin and A. F. Huxley. A quantitative description of membrane current and its application to conduction and excitation in nerve. *The Journal of Physiology*, 117(4):500–544, 1952.
- [64] E. N. Lorenz. Deterministic nonperiodic flow. *Journal of Atmospheric Sciences*, 20(2):130–141, 1963.
- [65] K. He, X. Zhang, S. Ren, and J. Sun. Deep residual learning for image recognition. *arXiv.org [Preprint]*, 2015. <https://arxiv.org/abs/1512.03385>.
- [66] M. H. Holmes. *Introduction to the Foundations of Applied Mathematics*. Springer, Cham, 2019.
- [67] N. K. Madsen. The method of lines for the numerical solution of partial differential equations. *SIGNAL Newsl.*, 10(4):5–7, 1975.

Supplementary Materials:

Integrating Physics-Informed Deep Learning and Numerical Methods for Robust Dynamics Discovery and Parameter Estimation

Caitlin Ho, Andrea Arnold*

Department of Mathematical Sciences, Worcester Polytechnic Institute, Worcester, MA, USA

* Corresponding author: anarnold@wpi.edu, ORCID 0000-0003-3003-882X

S1 Comparing Various LMM Schemes

As described in Section 3, we carefully choose the time and spatial discretizations for the three examples in the numerical results according to the absolute stability regions of the numerical methods employed. Recall that the general form of an M -step linear multistep method (LMM) is given by

$$\sum_{j=0}^M \alpha_j \mathbf{x}_{n+j} = \Delta t \sum_{j=0}^M \beta_j \mathbf{f}(t_{n+j}, \mathbf{x}_{n+j}) \quad (\text{S1})$$

where $\mathbf{x}_n \approx \mathbf{x}(t_n)$ and different choices for the coefficients α_j, β_j characterize different families of LMMs. When $\beta_M = 0$, the method is said to be *explicit*; otherwise it is *implicit*. Explicit schemes are straightforward to implement since the computation of \mathbf{x}_{n+M} depends only on the previous values $\mathbf{x}_{n+M-1}, \dots, \mathbf{x}_n$ (and possibly the RHS function values at these points), while implicit schemes rely also on $\mathbf{f}(t_{n+M}, \mathbf{x}_{n+M})$ and thereby require the solution of an optimization problem at each step. Figure S1 plots the absolute stability regions for the first five methods of the three main LMM families: Adams-Bashforth (AB), Adams-Moulton (AM), and the backwards differentiation formulae (BDF).

To evaluate the performance of the proposed methods across different LMM schemes, we conduct several numerical experiments comparing the resulting state predictions for both the dynamics discovery approach in Section 2.1 and parameter estimation problem in Section 2.2 using the same setup described in these sections. In particular, we compare results across the 2-step schemes AB2 (explicit), AM2 (implicit), and BDF2 (implicit) on the FitzHugh-Nagumo example outlined in Section 3.1 with noiseless data. For the problems at hand, we note that 2-step methods provide a reasonable balance between computational efficiency and accurate results. Figure S2 and Table S1 display the comparison results for the dynamics discovery problem, while Figure S3 and Tables S2 and S3 show the results for the parameter estimation problem.

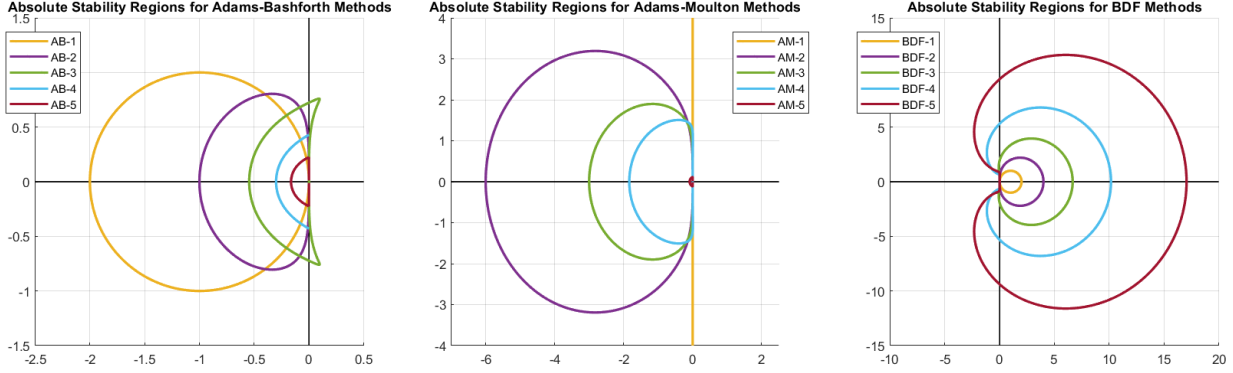


Figure S1: Absolute stability regions of the LMM schemes (from left to right): explicit Adams-Bashforth methods AB1-5; implicit Adams-Moulton methods AM1-5; and implicit backward differentiation formulae BDF1-5. Note that the stability region of AM1 corresponds to the left half of the complex plane, and the BDF stability regions are defined by the areas exterior to the curves.

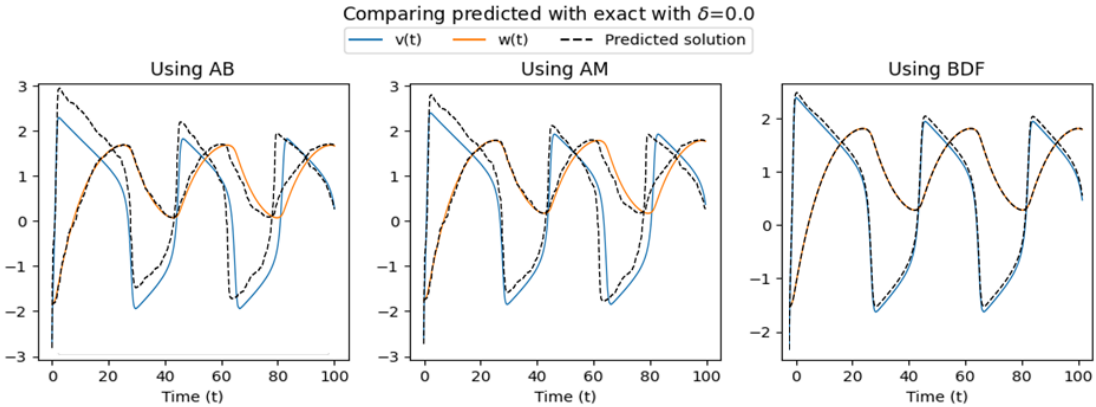


Figure S2: Dynamics discovery model predictions of the FitzHugh-Nagumo model using various LMM 2-step schemes with noiseless observed data.

From the results in Table S1, BDF2 appears to have the most accurate and efficient performance for the dynamics discovery problem. We also observe closer model predictions of dynamics in Figure S2 when using BDF2. When comparing the model predictions for the parameter estimation approach in Figure S3, there is not much difference between the three numerical methods, except at around $t \in [90, 100]$. For the learned physical parameters, we observe similar results as discussed in Section 4, with some unchanged values and fairly high relative errors. However, when we compare the MSE and computation time in Table S2, AB2 provides a reasonable balance between accuracy and efficient performance. From this analysis, we conclude that BDF2 and AB2 are suitable LMM choices for the examples in Sections 3.1.1 and 3.1.2. We also experimented with various choices for the number of steps M , but based on empirical evidence, the 2-step methods best balanced the trade-off between computational efficiency and accurate predictions out of all the methods we considered.

	MSE		Training Time (min)
	v	w	
AB2	4.77e-01	2.78e-02	28.86
AM2	3.64e-01	2.75e-02	59.16
BDF2	9.12e-03	3.31e-06	21.84

Table S1: Comparing various LMM 2-step scheme MSEs and computational time for the FitzHugh-Nagumo model dynamics discovery problem.

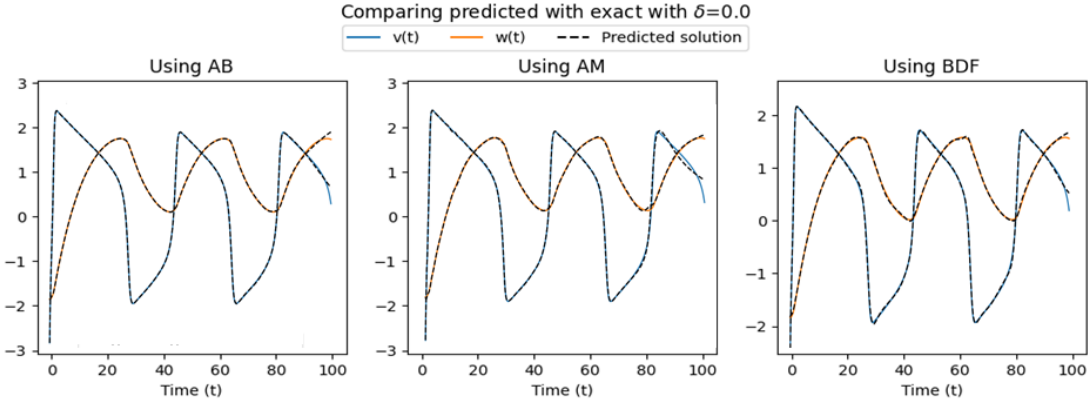


Figure S3: Parameter estimation model predictions of the FitzHugh-Nagumo model using various LMM 2-step schemes with noiseless observed data.

	MSE		Training Time (min)	
	v	w	Pre-training	Fine-tuning
AB2	7.54e-04	4.01e-04	2.77	10.17
AM2	3.29e-03	4.82e-04	4.53	10.04
BDF2	1.32e-03	5.08e-04	3.00	10.88

Table S2: Comparing various LMM 2-step scheme MSEs and computational time for the FitzHugh-Nagumo model parameter estimation problem.

	Parameter	True Value	Initial Value	Estimated Value	Relative Error
AB2	a	0.7	0.510	0.510	0.272
	b	0.8	0.625	0.625	0.219
	c	12.5	13.667	12.897	0.032
	z	1	0.876	0.876	0.124
AM2	a	0.7	0.292	0.751	0.073
	b	0.8	0.862	0.862	0.078
	c	12.5	13.732	12.116	0.031
	z	1	0.703	0.917	0.083
BDF2	a	0.7	0.901	0.897	0.281
	b	0.8	0.863	0.863	0.079
	c	12.5	13.454	12.402	0.008
	z	1	0.813	0.813	0.187

Table S3: Comparing estimated physical parameter values from the FitzHugh-Nagumo model with noiseless observed data for various LMM 2-step schemes.